Parallel direct laser writing in three dimensions with spatially dependent aberration correction

Alexander Jesacher[1,*] **and Martin J. Booth**[2,3]

[1]*Division of Biomedical Physics, Innsbruck Medical University, Müllerstraße 44, 6020 Innsbruck, Austria*

[2]*Department of Engineering Science, University of Oxford, Parks Road, Oxford, OX1 3PJ, United Kingdom*

[3]*Martin.Booth@eng.ox.ac.uk*

[*]*AlexanderJesacher@i-med.ac.at*

Abstract: We propose a hologram design process which aims at reducing aberrations in parallel three-dimensional direct laser writing applications. One principle of the approach is to minimise the diffractive power of holograms while retaining the degree of parallelisation. This reduces focal distortion caused by chromatic aberration. We address associated problems such as the zero diffraction order and aberrations induced by a potential refractive index mismatch between the immersion medium of the microscope objective and the fabrication substrate. Results from fabrication in diamond, fused silica and lithium niobate are presented.

OCIS codes: (140.3390) Laser materials processing; (070.6120) Spatial light modulators; (050.1970) Diffractive optics; (090.1000) Aberration compensation

References and links

1. S. Wong, M. Deubel, F. Pérez-Willard, S. John, G. A. Ozin, M. Wegener, and G. von Freymann, "Direct Laser Writing of Three-Dimensional Photonic Crystals with a Complete Photonic Bandgap in Chalcogenide Glasses," Adv. Mater. **18,** 265–269 (2006).
2. G. D. Marshall, M. Ams, and M. J. Withford, "Direct laser written waveguide Bragg gratings in bulk fused silica," Opt. Lett. **31,** 2690–2691 (2006).
3. G. Della Valle, R. Osellame and P. Laporta, "Micromachining of photonic devices by femtosecond laser pulses," J. Opt. A **11,** 013001 (18pp) (2009).
4. C. Mauclair, G. Cheng, N. Huot, E. Audouard, A. Rosenfeld, I. V. Hertel, and R. Stoian, "Dynamic ultrafast laser spatial tailoring for parallel micromachining of photonic devices in transparent materials," Opt. Express **17,** 3531–3542 (2009).
5. M. Pospiech, M. Emons, A. Steinmann, G. Palmer, R. Osellame, N. Bellini, G. Cerullo, and U. Morgner, "Double waveguide couplers produced by simultaneous femtosecond writing," Opt. Express **17,** 3555–3563 (2009).
6. M. Sakakura, T. Sawano, Y. Shimotsuma, K. Miura, and K. Hirao, "Fabrication of three-dimensional 1 x 4 splitter waveguides inside a glass substrate with spatially phase modulated laser beam," Opt. Express **18,** 12136–12143 (2010).
7. M. S. Rill, C. Plet, M. Thiel, I. Staude, G. Freymann, S. Linden, and M. Wegener, "Photonic metamaterials by direct laser writing and silver chemical vapour deposition," Nature Materials **7,** 543–546 (2009).
8. Y. Y. Cao, N. Takeyasu, T. Tanaka, X. M. Duan, and S. Kawata, "3D Metallic Nanostructure Fabrication by Surfactant-Assisted Multiphoton-Induced Reduction," Small **5,** 1144–1148 (2009).
9. J. K. Gansel, M. Thiel, M. S. Rill, M. Decker, K. Bade, V. Saile, G. v. Freymann, S. Linden, and M. Wegener, "Gold Helix Photonic Metamaterial as Broadband Circular Polarizer," Science **325,** 1513 (2009).
10. S. Maruo, O. Nakamura, and S. Kawata, "Three-dimensional microfabrication with two-photon-absorbed photopolymerization," Opt. Lett. **22,** 132–134 (1997).
11. K. S. Lee, D. Y. Yang, S. H. Park, and R. H. Kim, "Recent developments in the use of two-photon polymerization in precise 2D and 3D microfabrications", Polym. Adv. Technol. 17, 72–82 (2006).

#133208 - $15.00 USD Received 10 Aug 2010; revised 13 Sep 2010; accepted 16 Sep 2010; published 21 Sep 2010

12. Y. Kuroiwa, N. Takeshima, Y. Narita, S. Tanaka, and K. Hirao, "Arbitrary micropatterning method in femtosecond laser microprocessing using diffractive optical elements," Opt. Express **12,** 1908–1915 (2004).
13. J.-I. Kato, N. Takeyasu, Y. Adachi, H.-B. Sun, and S. Kawata, "Multiple-spot parallel processing for laser micronanofabrication," Appl. Phys. Lett. **86,** 044102 (2005).
14. S. Hasegawa, Y. Hayasaki, and N. Nishida, "Holographic femtosecond laser processing with multiplexed phase Fresnel lenses," Opt. Lett. **31,** 1705–1707 (2006).
15. M. Yamaji, H. Kawashima, J. Suzuki, and S. Tanaka,"Three dimensional micromachining inside a transparent material by single pulse femtosecond laser through a hologram," Appl. Phys. Lett. **93,** 041116 (2008).
16. G. Mínguez-Vega, J. Lancis, J. Caraquitena, V. Torres-Company, and P. Andrés, "High spatiotemporal resolution in multifocal processing with femtosecond laser pulses," Opt. Lett. **31,** 2631–2633 (2006).
17. D. Palima and V. Ricardo Daria, "Holographic projection of arbitrary light patterns with a suppressed zero-order beam," Appl. Opt. **46,** 4197–4201 (2007).
18. R. W. Gerchberg and W. O. Saxton, "A practical algorithm for the determination of phase from image and diffraction plane pictures," Optik **35,** 227-246 (1972).
19. R. Di Leonardo, F. Ianni, and G. Ruocco, "Computer generation of optimal holograms for optical trap arrays," Opt. Express **15,** 1913–1922 (2007).
20. J. Bengtsson, "Kinoform design with an optimal-rotation-angle method," Appl. Opt. **33,** 6879-6884 (1994).
21. P. Török, P. Varga, Z. Laczik and G. R. Booker "Electromagnetic diffraction of light focused through a planar interface between materials of mismatched refractive indices: an integral representation," J. Opt. Soc. Am. A **12,** 325–331 (1995).
22. M. J. Booth, M. A. A. Neil and T. Wilson, "Aberration Correction for Confocal Imaging in Refractive Index Mismatched Media," J. Microsc. **192,** 90–98 (1998).
23. S. Stallinga, "Light distribution close to focus in biaxially birefringent media," J. Opt. Soc. Am. A **21,** 1785-1798 (2004).

1. Introduction

Direct laser writing (DLW) is a promising technique for the creation of photonic devices at the micro scale. Applications range from fabricating artificial bandgap materials [1] to waveguide-based devices [2, 3, 4, 5, 6] and metal nanostructures [7, 8, 9]. DLW commonly employs a powerful short-pulsed laser system to write the required structures directly into the target material, which can be a metallic or dielectric solid or a liquid resin in the case of two-photon polymerisation [10, 11]. A drawback of DLW is its sequential character. In contrast to lithographic techniques, where whole areas are exposed simultaneously, in DLW structures have to be written one after another by the focused laser. Nevertheless, higher fabrication speeds are necessary if DLW is to become a practical prospect for industrial manufacturing, or for the fabrication of larger devices. To overcome this limitation, parallel processing techniques have been proposed and demonstrated [12, 13, 14, 15]. Such methods typically rely on diffractive elements or micro lens arrays to divide the laser beam into multiple sub-beams. The use of diffractive elements however can be problematic for ultrashort laser pulses in the femto-second regime. The bandwidth of these lasers is non-negligible; for example, a titanium sapphire 100 fs pulsed laser at centre wavelength 790nm has a bandwidth of approximately 15 nm or 1.9% of the centre wavelength (measured values for our system). Chromatic dispersion therefore degrades the focus, especially for foci at large distance from the optical axis; these are elongated in the radial direction and show a correspondingly reduced peak intensity. Although there is an effective way to compensate chromatic aberration to a certain extent by incorporating further diffractive elements [16], it might not always be practicable due to accompanying higher losses and the higher degree of experimental complexity.

We propose a practical approach for parallel direct laser writing which aims at reducing chromatic aberration by choosing a specific hologram design. In this design, the diffractive power of the hologram (and hence chromatic aberration) is minimised by encoding only foci close to the centre, i.e. the point where an undiffracted beam would focus. Figure 1a) illustrates the idea. It sketches two different parallel fabrication techniques for building up a three-dimensional body-centred cubic (BCC) lattice of point-like material modifications in a dielectric material. These

#133208 - $15.00 USD Received 10 Aug 2010; revised 13 Sep 2010; accepted 16 Sep 2010; published 21 Sep 2010

modifications should henceforth be referred to as “voxels”. In the first method (left), a whole two-dimensional layer of voxels (blue coloured spots) is encoded in a single hologram, such that a single laser exposure forms a whole layer of them. In this manner, the entire lattice is fabricated layer by layer. The voxels at larger distances from the axis appear elongated due to chromatic aberration. In the second approach, a three-dimensional arrangement of spots is encoded in a single hologram and the whole crystal is built up by multiples of these elementary building blocks. Although both approaches require the same number of laser pulses for completing the entire crystal structure, the second one suffers far less from chromatic aberration. Furthermore, the diffraction efficiency of the 3D hologram is significantly higher compared to the 2D approach. The idea appears simple, nevertheless two obstacles have to be overcome in order to make it practicable: Firstly, fabricating close to the optical axis requires an effective compensation of the zero diffraction order which forms a focal spot in the centre of the fabrication space. The zero order results from imperfections of the diffractive structure and can have significant strength for complicated diffractive structures that encode dozens of spots. Secondly, in almost all practical cases a refractive index mismatch is present between the immersion medium of the objective lens and the fabrication substrate. This introduces a depth-dependent spherical aberration (SA), because axial rays of the focussing cone converge at a different axial position than marginal rays. This effect is sketched in Fig. 1b). Therefore, a proper hologram design should consider individual aberration correction factors for all the distinct layers that are encoded in a single hologram.

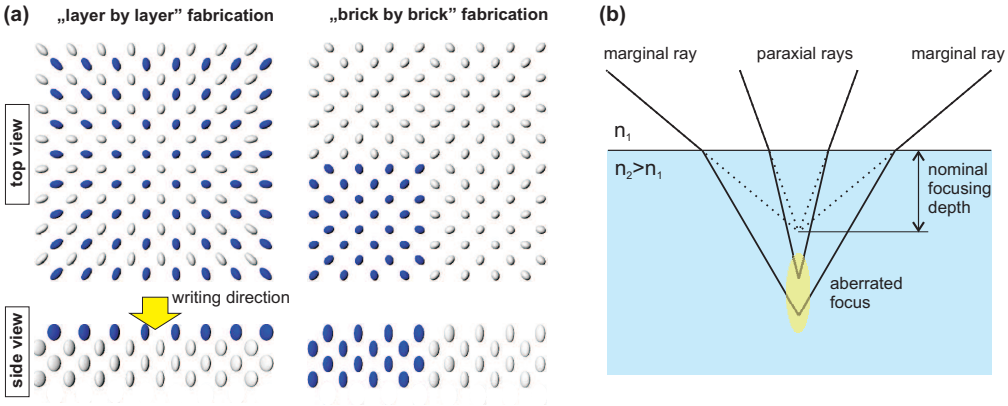

Fig. 1. a) Building a three-dimensional BCC lattice with parallel direct laser writing techniques. The formation of three-dimensional building blocks (right) reduces chromatic aberration-induced elongation of defects compared to the “layer by layer” technique (left). The corresponding elementary building blocks which are created with a single laser pulse are depicted in blue. b) Focusing through a refractive index mismatch: marginal rays focus at a different depth than paraxial rays – this elongates the focal spot and represents a spherical aberration.

In this paper we show how both obstacles can be addressed. We experimentally demonstrate the efficient suppression of the zero diffraction order by an appropriate hologram design. Methods to achieve this are routinely used in the design of static diffractive optical elements, but have only recently been experimentally demonstrated for a dynamic spatial light modulator [17]. Furthermore, we show how a hologram design algorithm can be modified in order to tackle the problems caused by SA originating from a refractive index mismatch. This opens the door to aberration-free single-shot fabrication in three dimensions. We present experimental results confirming the effectiveness of our method.

#133208 - $15.00 USD Received 10 Aug 2010; revised 13 Sep 2010; accepted 16 Sep 2010; published 21 Sep 2010

2. Hologram design

The algorithm we use is based on a Gerchberg-Saxton algorithm [18], which is optimized to produce multiple spots of high uniformity. It has recently been introduced as *weighted Gerchberg-Saxton* method (GSW) in the context of optical trapping [19]. A similar approach – the *optimal-rotation-angle* (ORA) method – has been introduced by Jörgen Bengtsson in 1994 [20]. Our considerations follow the work of Di Leonardo et al. [19], with adaptations to satisfy the specific requirements of our application.

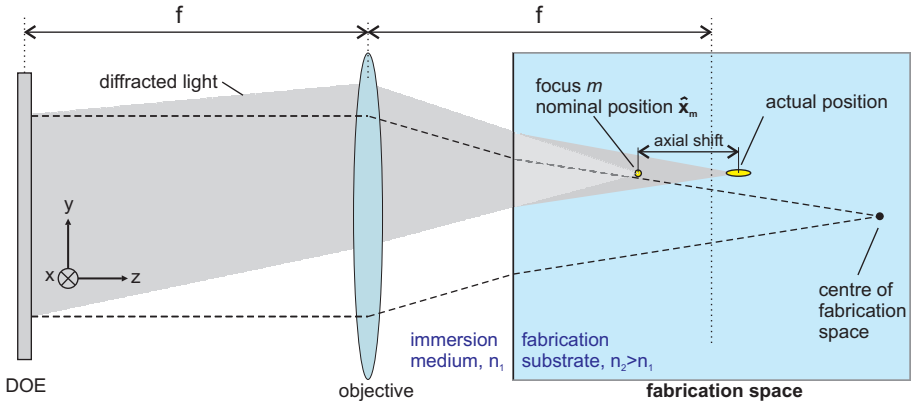

Fig. 2. Shaping a focus inside of a fabrication substrate with a diffractive optical element. f is the focal length of the objective lens.

Let us consider that we would like to shape a number of M equally bright foci in the far field using a phase diffractive optical element (DOE). This situation is sketched in Fig. 2 (only one focus shown). There, a lens acts as Fourier transformer, i.e. the field in its back focal plane is the Fourier transform of the field in the DOE plane. The presence of the fabrication substrate elongates the focus and shifts it towards larger depths if its refractive index exceeds that of the immersion medium. Each focus m has an assigned *nominal* position $\hat{\mathbf{x}}_\mathbf{m} = (\hat{x}_m, \hat{y}_m, \hat{z}_m)$ in the fabrication space, which differs from the *actual* position because of the refraction at the substrate surface. According to diffraction theory, the field at each focus can be expressed as a sum over the fields in every DOE pixel, considering individual propagator functions $\Delta_m(x,y)$:

$$V_m = \sum_{\mathbf{x}} \frac{1}{N} \exp\left[i\Phi(x,y) - i\Delta_m(x,y)\right]. \tag{1}$$

Here, $\Phi(x,y)$ is the phase function of the DOE and N its total number of pixels. In the above expression, some non-relevant constants have been neglected, which is why V_m does not truly represent the electric field strength. The propagator functions $\Delta_m(x,y)$ can be defined as:

$$\Delta_m(x,y) = \frac{2\pi}{\lambda_0 f}\left(x\hat{x}_m + y\hat{y}_m\right) + \hat{z}_m\left[D(x,y) + SA(x,y)\right], \tag{2}$$

where $D(x,y)$ is a defocus term which determines the axial position of the focus and $SA(x,y)$ the expression which leads to a compensation of the SA due to a refractive index mismatch. λ_0 is the laser wavelength in vacuum and f the focal length of the objective. The defocus function is frequently defined in the paraxial approximation as a radially quadratic phase function. However, for microscope objectives designed to fulfil the sine condition, the defocus function should be spherical rather than parabolic. This is especially important for objectives with high

#133208 - $15.00 USD Received 10 Aug 2010; revised 13 Sep 2010; accepted 16 Sep 2010; published 21 Sep 2010

numerical apertures (NA). When transformed into the pupil plane, the defocus phase per unit axial displacement can be defined as:

$$D_{n_1}(r) = \frac{2\pi}{\lambda_0 f}\sqrt{f^2 n_1^2 - r^2}, \tag{3}$$

where n_1 is the refractive index of the immersion medium and $r = (x^2 + y^2)^{1/2}$ represents the radial coordinate. The subscript n_1 indicates that the function represents a spherical wavefront in the immersion medium. The spherical aberration compensation function per unit axial displacement can be defined as [21, 22]

$$\begin{aligned} SA(r) &= -\frac{2\pi}{\lambda_0 f}\left[\sqrt{f^2 n_2^2 - r^2} - \sqrt{f^2 n_1^2 - r^2}\right] \\ &= D_{n_1}(r) - D_{n_2}(r), \end{aligned} \tag{4}$$

where n_2 represents the refractive index of the target medium. It is apparent that for $n_1 = n_2$ (no refractive index mismatch), $SA(r)$ assumes the value zero. Commonly, the defocus and spherical aberration functions are defined using normalised coordinates rather than real ones; corresponding definitions can be found in the Appendix. It should be noted that the correction term $SA(r)$ entirely removes the effects of the refraction at the material interface, i.e., it repairs the focus distortion *and* moves the spot back to its nominal position $\hat{\mathbf{x}}_\mathbf{m}$. For our experiments however we decided only to compensate that part of $SA(r)$ which is responsible for the focus distortion. This eases the demands on the modulation bandwidth of the DOE. As a consequence the resulting spot distribution in the fabrication space will be axially stretched. An explanation how the corresponding part can be extracted from $SA(r)$ can be found in the Appendix.

The algorithm may start with a random DOE phase function $\Phi(x,y)$. Then, for each spot m in the fabrication space, the values V_m are derived according to Eq. (1). Based on these values, one iteration is completed by calculating an updated version of $\Phi(x,y)$ as follows:

$$\Phi(x,y) = \arg\left[\sum_m \exp\left[i\Delta_m(x,y)\right] \frac{V_m}{|V_m|} w_m\right]. \tag{5}$$

In this equation, w_m is a weighting factor which leads to a very high spot uniformity. In the first iteration ($k = 0$), w_m takes the value 1. For every following iteration, it is defined as:

$$w_m^k = w_m^{k-1} \frac{\langle |V_m^{k-1}| \rangle_m}{|V_m^{k-1}|}, \tag{6}$$

with k being the iteration number. The function $\langle . \rangle_m$ returns the average field magnitude. In this manner, intensities of spots that are too strong are reduced in the following iteration, while those of weaker spots are enhanced.

It should be mentioned that in our case a weighting factor as defined in Eq. (6) will only lead to high uniformities amongst sets of spots lying in equal depth. There will be a trend to higher spot intensities with increasing depth. We found that this effect was negligible in our experiments. If required, it could be compensated by including a z-dependent correction term into the definition of w_m.

3. Experimental set-up and results

Figure 3(a) shows a sketch of the experimental set-up. The pulses emitted from the regeneratively amplified titanium sapphire laser (*Solstice*, Newport/Spectra Physics, 100 fs pulse duration, 1 kHz repetition rate, 790 nm centre wavelength) were attenuated using a rotatable half

#133208 - $15.00 USD Received 10 Aug 2010; revised 13 Sep 2010; accepted 16 Sep 2010; published 21 Sep 2010

wave plate and a Glan-Taylor polariser. The beam was expanded and directed to a reflective liquid crystal SLM (*X10468-02*, Hamamatsu Photonics), which was used to display the phase holograms. The SLM was imaged onto the objective pupil. The specimen was located on a 3D piezo stage (*Tritor102SG*, Piezosystem Jena) which provided up to 100 μm translation in all axes. The system incorporated a LED illuminated transmission microscope for observing the specimen.

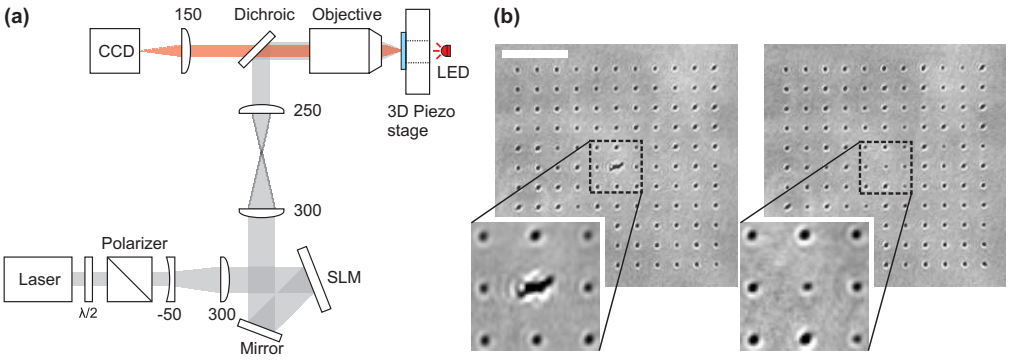

Fig. 3. a) Experimental set-up. Lens focal lengths are in mm. b) Suppression of the Zero Order. The images show 2D lattices of voxels, written into lithium niobate with single laser pulses. Left: The zero order light leads to a very pronounced defect at the centre. The defect appears elongated, which results from aberrations caused by the uneven SLM surface. Right: The intensity of the zero order has been compensated by fine-tuning amplitude and phase of the central spot. The scale bar corresponds to 10 μm.

To suppress the zero diffraction order of diffractive optical elements, one extra spot can be incorporated into the hologram design, the only purpose of which is to destructively interfere with the zero order light. The amplitude and phase of this extra spot have to be carefully chosen, and represent additional constraints in the hologram design. Figure 3(b) summarises experimental results of active zero order suppression. It shows two images of two-dimensional lattices, written into lithium niobate by single laser pulses using an Olympus oil immersion objective (60x, 1.4*NA*). The lattice in the left image was produced using an ordinary on-axis hologram, which has been derived using the algorithm described in the previous section. The hologram used to produce the lattice on the right was derived incorporating active zero order compensation. There, the properties of the central spot were fine-tuned to reduce the zero order intensity. Amplitude and phase magnitudes of the central spot were experimentally determined. To determine the amplitude, the position of the compensation spot was first chosen to be slightly off-axis, such that it focused adjacently to the zero order. Then the brightness of the compensation spot was adapted until the voxels produced by the compensation spot and the zero order looked identical. To determine the optimal phase, the compensation spot was overlapped with the zero order and its phase value changed until the zero order was optimally suppressed. For most SLMs, to compensate their surface unevenness, it is necessary to add a corrective phase pattern $C(x,y)$ to the final hologram before it is displayed. This was also done for all experiments reported in this paper. If such a pattern is used one must subtract it from the phase of the compensation spot, so that it is affected by the same aberrations as the zero order. Otherwise, full suppression of the zero order is not possible. Hence the propagator function of the compensation spot should be of the form $\Delta(x,y) = -C(x,y)$.

Next, to demonstrate the effectiveness of the implemented SA correction, we calculated holograms of identical structures with and without correction term $SA(r)$. Figure 4 shows axial helices written in monocrystalline diamond (Element Six, UK) and fused silica (Schott Lithosil

#133208 - $15.00 USD Received 10 Aug 2010; revised 13 Sep 2010; accepted 16 Sep 2010; published 21 Sep 2010

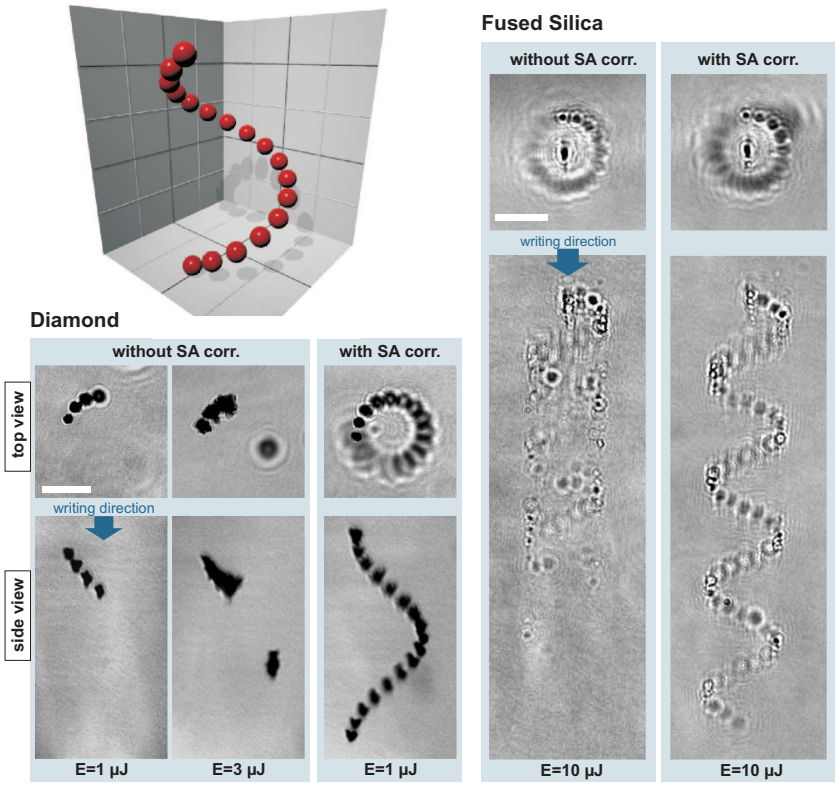

Fig. 4. Helical structures written into diamond and fused silica using single holograms; upper left corner: 3D model of the structure written into diamond; lower left box: fabrication in diamond – the images show results of holograms which were designed with and without integrated SA compensation; laser pulse energies are stated below the images; right box: helical structures written into fused silica, with and without SA correction; the scale bars correspond to 10 μm.

Q0), respectively. Shown is a 3D model of the diamond helix as well as top and side views of the fabricated structures. Each writing process consisted of 50 subsequent laser pulses. The used pulse energies are stated below the figures and refer to values before the objective lens. The objectives used were an Olympus oil immersion objective (60x, 1.4*NA*) for writing in diamond and an Olympus air objective (40x, 0.95*NA*) for fused silica. For our system parameters, the corresponding RMS aberration magnitudes per micrometre nominal focusing depth are around 1.05 rad for diamond and 0.70 rad for fused silica. These numbers refer to the total aberration as described by Eq. (5). As mentioned earlier, we only correct the part of $SA(r)$ which is responsible for the focus distortion. This part has a RMS magnitude of 0.24 rad for diamond and 0.18 rad for fused silica. The diamond helix has a diameter of 14 μm and is composed out of 17 distinct spots arranged in a single round-trip. The nominal axial extension of the whole structure is 20 μm, but was extended to approximately 30 μm by the refocussing effect of the refractive index mismatch (n_1=1.52, n_2=2.42). It is apparent from Fig. 4 that without incorporating SA correction only the first few spots of the helix could be created, whereas the formation of deeper ones was inhibited by aberrations. Interestingly, even increasing the pulse energy by a factor of three did not lead to a production of the whole structure, but lead to enlargement and fusion of the first few spots instead. A contributing factor to this phenomenon could be the fact that

#133208 - $15.00 USD Received 10 Aug 2010; revised 13 Sep 2010; accepted 16 Sep 2010; published 21 Sep 2010

the defects produced in diamond are strongly light absorbing and thus counteract the formation of further defects by absorbing/scattering the incident beam. On the contrary, incorporating the SA term in the hologram computation led to fabrication of the complete helix with relatively high spot uniformity.

A similar experiment was performed in fused silica. There, structures reaching as far as 100 μm deep into the glass could be produced without problems. The example structure is again a helix, this time consisting out of 68 spots in four revolutions. The diameter of this helix is 12 μm and its nominal helical pitch 20 μm. The helix written into fused silica is obviously less axially stretched than the diamond-helix, which is due to the less severe refractive index mismatch (n_1=1, n_2=1.45). When comparing the helices in diamond and fused silica, it becomes apparent that the latter one is accompanied by a pronounced central defect, which was caused by the zero order, whereas the diamond-helix shows no such "extra voxel" on the optical axis. The reason for this is that the hologram of the diamond-helix encodes fewer spots. Each of those spots was more intense than the zero diffraction order, the intensity of which lay below the fabrication threshold.

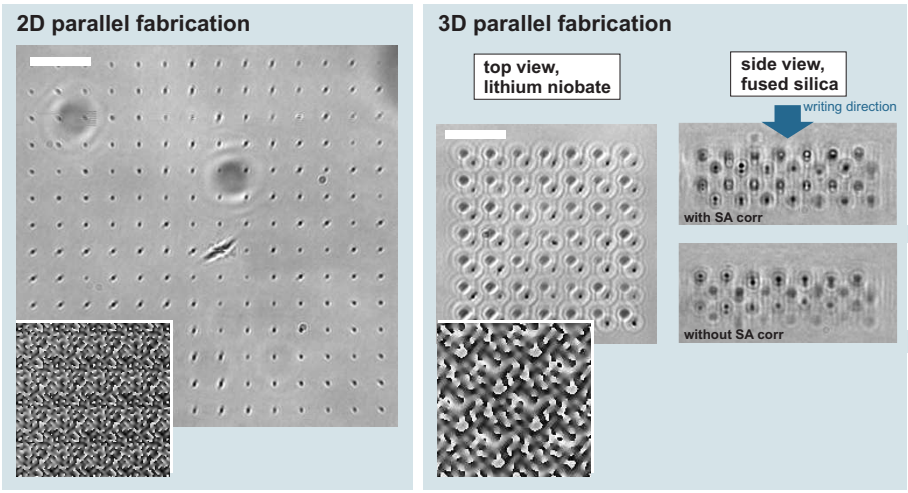

Fig. 5. Fabrication of two- and three-dimensional crystal structures with single holograms. Left box: 14×14 array of voxels in lithium niobate. The inset shows a part of the corresponding hologram. Right box: Top view of a 7×7×4 lattice in lithium niobate, focused onto the topmost layer. The hologram used is again shown as inset. Side views of identical structures in fused silica are shown on the right. The lattices in fused silica were produced with (upper image) and without SA-corrected holograms. The scale bars correspond to 10 μm.

Finally, we aimed to produce three-dimensional lattice structures using a single hologram. We fabricated two- and three-dimensional BCC lattices with a lattice constant of 4.5 μm in lithium niobate (X-cut) using the Olympus oil objective. The sample was rotated such that the linear laser polarisation closely matched the ordinary mode, which does not suffer from additional birefringence-induced astigmatism [23]. Both structures consisted of 196 spots. Figure 5 compares the outcomes. The left image shows the 2D layer – a 14×14 grid of voxels – written by 50 subsequent pulses of 4.7 μJ energy. Clearly, the defects become more elongated with increasing distance from the centre. Note that in this experiment no zero order compensation was performed, hence the presence of the central distorted feature. The large image in the right box shows a 7×7×4 BCC lattice, written by a train of 50 pulses of only 3.7 μJ energy. The

#133208 - $15.00 USD Received 10 Aug 2010; revised 13 Sep 2010; accepted 16 Sep 2010; published 21 Sep 2010

3D hologram diffracted more efficiently than the 2D hologram, which explains that less energy was required to produce voxels of comparable strength. The radial distortion was apparently less pronounced than in the previous experiment. From this view, it was not however clear whether all layers have been fabricated in similar quality. We therefore produced the same 3D lattice with the Olympus air objective in fused silica. The fused silica substrate had multiple polished facets, permitting observation of the fabricated structures from a direction perpendicular to the optic axis of the fabrication system. This allowed inspecting the lower lattice layers by means of taking images from the side (smaller images in the right box). Comparing direct laser writing in lithium niobate and fused silica is legitimate in our case, since similar aberration magnitudes are introduced in both cases (0.18 rad/μm by fused silica with the dry lens and 0.23 rad/μm for the ordinary mode by lithium niobate using the oil immersion objective). The side-views show "BCC-bricks" fabricated with and without SA correction. Especially for the lowest layer, a clear contrast difference between the two cases is noticeable. The insets in Fig. 5 show parts of the phase holograms for each case.

So far, our results show that with three-dimensional parallel laser writing, hundreds of defects can be shaped without significant dispersion affecting the fabrication quality. This is a consequence of the comparatively low diffractive power of the corresponding holograms. Another positive side effect of this is the higher diffraction efficiency. For both fundamental and practical reasons, the efficiency of SLM-based holograms drops with increasing spatial frequency content. According to the manufacturer, the diffraction efficiency of our device for instance is 88% for a blazed grating with a period of 16 pixels but only around 22% for a 2-pixel-grating (corresponding to 25 lines per mm).

4. Discussion and summary

From Eqs. (2) and (7) one sees that lateral and axial chromatic aberration have equal impact, i.e. a percent increase of the wavelength results in a percent increase of the lateral and axial distances between focus position and the fabrication space centre. This suggests that – in order to minimise chromatic aberration – ideally one should design a 3D structure that is spherically symmetric. If one considers the defocussing effect of a refractive mismatch however, which leads to an axial stretch, one finds that the ideal shape is an axially prolate ellipsoid. It should be noted, however, that for the purpose of building extended structures from elementary building blocks as indicated in Fig. 1, the shape of a building block should be chosen such that the presence of an existing block does not affect the production of another one adjacent to it. Problems could occur as the light incident to the focal region at high inclinations to the optic axis could pass through existing fabricated structures. For block-shaped fabrication cells – depending on the target material and the *NA* of the objective – this precondition will restrict the thickness of a cell roughly to the distance between two adjacent cells. A solution to this problem is to use multiple unit cells with appropriate shapes, e.g. blocks with chamfered edges, which are alternately fabricated to build up the complete structure.

In summary, we proposed a strategy for parallel direct laser writing applications, which aims to reduce problems induced by chromatic aberration. The basic idea is that the diffractive power of the DOE should be minimised by encoding only spots in closest vicinity to the centre of the fabrication space. This however requires that, firstly, structures should be fabricated on axis and, secondly, should be designed exploiting three dimensions rather than two. We presented solutions to two accompanying problems, namely the presence of the zero diffraction order and the fact that three-dimensional structures require a hologram design algorithm which considers individual depth-dependent aberration correction factors. We demonstrated the effectiveness of our strategy by means of various experiments conducted in diamond, fused silica and lithium niobate.

#133208 - $15.00 USD Received 10 Aug 2010; revised 13 Sep 2010; accepted 16 Sep 2010; published 21 Sep 2010

5. Appendix

Equations (3) and (5) express the defocus and spherical aberration functions in real length coordinates. These definitions require knowledge of the objective focal length f, which can be obtained by dividing the focal length of the manufacturer's standard microscope tube lens (180 mm for Olympus) by the objective magnification. A more common definition uses normalised coordinates. The radial coordinate r is expressed in units of the objective pupil radius, which is obtained by multiplying f with NA. Using this normalised radius $\rho = r/(f\ NA)$, Eqs. (3) and (5) take the following forms:

$$D_{n_1}(\rho) = \tfrac{2\pi}{\lambda_0} NA \sqrt{\tfrac{n_1^2}{NA^2} - \rho^2}, \tag{7}$$

$$SA(\rho) = -\tfrac{2\pi}{\lambda_0} NA \left[\sqrt{\tfrac{n_2^2}{NA^2} - \rho^2} - \sqrt{\tfrac{n_1^2}{NA^2} - \rho^2} \right]. \tag{8}$$

It should be noted that the functions $SA(\rho)$ and $D_{n_1}(\rho)$ are sampled representations of the continuous functions defined above. In practice, the sampling is performed on a regular Cartesian grid corresponding to the pixels of the SLM.

To obtain the part of $SA(r)$ responsible for the focus distortion, one must remove the total amount of defocus it contains. In analogy to vector analysis this operation can be expressed as:

$$\hat{SA}(r) = SA(r) - \frac{\langle SA'(r), D'_{n_2}(r) \rangle}{\langle D'_{n_2}(r), D'_{n_2}(r) \rangle} D_{n_2}(r). \tag{9}$$

Here, $\hat{SA}(r)$ denotes the "defocus-free" spherical aberration and $\langle .,. \rangle$ defines an inner product:

$$\langle SA'(r), D'_{n_2}(r) \rangle = \frac{1}{N} \sum_{\mathbf{r}} SA'(r) D'_{n_2}(r). \tag{10}$$

The functions $SA'(r)$ and $D'_{n_2}(r)$ represent spherical aberration and defocus with subtracted mean values:

$$SA'(r) = SA(r) - \tfrac{1}{N} \textstyle\sum_{\mathbf{r}} SA(r), \tag{11}$$

$$D'_{n_2}(r) = D_{n_2}(r) - \tfrac{1}{N} \textstyle\sum_{\mathbf{r}} D_{n_2}(r). \tag{12}$$

Acknowledgements

This work was supported by Engineering and Physical Sciences Research Council grants EP/E055818/1 and EP/H049037/1 and a research grant from Jesus College, Oxford.

#133208 - $15.00 USD Received 10 Aug 2010; revised 13 Sep 2010; accepted 16 Sep 2010; published 21 Sep 2010